VOL. 10, NO. 21, NOVEMBER 2015 ISSN 1819-6608
ARPN Journal of Engineering and Applied Sciences


www.arpnjournals.com

EFFECT OF SURFACE ROUGHNESS ON ADHESION STRENGTH IN ULTRASONIC SOLDERING OF GLASS

Mustafa M. Y., Hilmy I. and Adesta E. Y. T.
School of Materials and Manufacturing Engineering, Faculty of Engineering, International Islamic University Malaysia, Malaysia
E-Mail: my@royalselangor.com.my

ABSTRACT

The research focused on improving the adhesion strength of low melting temperature lead free solder to soda lime glass through ultrasonic soldering. This was conducted by analyzing the effect of glass surface roughness on shear separation strength and shear separation energy between glass and solders. Analysis was conducted through tensile stress test. Other soldering parameters involving temperature, time, vibration amplitude, solder alloys and frequency were kept constant. (Sn40Bi)0.3Mg and (Sn40Bi)0.5Al solder alloys were selected due to their low melting temperatures and good adhesion to glass. Shear separation strength and extension before fracture data from the tensile stress test was used to derive shear separation energy values. Solder adhesion strength and solder adhesion energy between solder alloys and glass improved with increasing glass surface roughness. Study on bonding mechanism was conducted by using scanning electron microscope (SEM) and energy dispersive X-ray spectroscopy (EDX). Bond between ultrasonic soldering of glass and solder alloys consists of metal oxide adhesion and mechanical adhesion.

Keywords: ultrasonic soldering, glass soldering, glass surface roughness; lead free solders; solder separation energy.

INTRODUCTION

The research focused on improving the adhesion strength of low melting temperature lead free solder to soda lime glass through ultrasonic soldering (US). This was conducted by analyzing the effect of glass surface roughness on shear separation strength and shear separation energy between glass and solders. Difficult to solder substrates may be bonded together using US method. Ultrasonic vibration induces micro cavitations on the surface of the substrate. Removal of oxide layer by micro cavitations allows surface wetting by suitable solder alloy. The mechanism for glass soldering is different as oxide layer removal is not a factor in adhesion. Research on bonding of glass and pewter (Sn5Sb1.2Cu by wt%) was conducted due to the requirement for strong bonding without using adhesive. Minimal gaps between substrates is necessary for strong adhesive bonding while molten solders can fill up the gaps naturally during US.

The adhesion strength of US is influenced by solder alloys, temperature, time, vibration amplitude and frequency. Solder alloys applicable for usage in US are dependent on the substrates. Al alloys substrates use Sn, Zn and Al as solder alloys. The adhesion strength depends on migration of Al and Al_2O_3 from substrates into the solder materials. US on 1070 Al alloy was conducted using Sn23Zn solder alloy [1]. Solder alloys Zn-Al and Zn-Sn were used for US of 5056 Al joints [2, 3]. Effects of soldering temperature and time on adhesion strength are mainly through increased diffusion and liquid fraction with formation of intermetallic compound (IMC) of solder alloys [2, 3]. [1, 4] demonstrated the optimum range of soldering time for 2024 Al substrate with Zn-Al and pure Sn filler metals. Longer solder time allows stronger adhesion through greater diffusion of Al and alumina into the filler metals. Adhesion strength for US is affected by vibrational amplitude. Solder joint for 1070 Al using Sn23Zn solder alloy was weakened when high vibrational amplitude squeezed out solders from gap between joint [5]. US frequency is dependent on the substrates. Frequency of 60 kHz was applied on glass and ceramics [6]. Frequency range of 40 kHz was applied on thermosonic bonding and US of amorphous metals [7 - 9]. Other applications of US were conducted at frequency of 19 - 21 kHz [2, 3, 5, 10, 11].

MATERIALS AND METHODS

(Sn40Bi)0.3Mg and (Sn40Bi)0.5Al solders with good adhesion property to glass were developed by the author by upgrading commercial solders Sn40Bi. Sn40Bi has low melting temperature with solidus temperature of 138°C and liquidus temperature of 170°C [12]. The low melting temperature is required for soldering glass and Sn5Sb1.2Cu without damaging the surface. Sn40Bi without addition of Mg and Al failed to adhere to glass during US as tested by the author. The mechanical properties, temperatures and chemical compositions data obtained for (Sn40Bi)0.3Mg and (Sn40Bi)0.5Al is shown in Table-1.

Table-1. Mechanical properties, temperatures and chemical compositions of (Sn40Bi)0.3Mg and (Sn40Bi)0.5Al solder alloys.

Properties	(Sn40Bi)0.3Mg	(Sn40Bi)0.3Mg
Temperatures		
Solidus (Ts)	141.6 °C	143.3 °C
Liquidus (Tl)	170.8 °C	171.1 °C
Mechanical		
Tensile strength	77.15 MPa	70.60 MPa
Elongation	6.18 %	5.40 %
Chemical compositions		
Sn	59.76	59.64
Bi	39.86	39.76
Mg	0.30	
Al		0.50
Others	Bal	Bal

Solder alloys (Sn40Bi)0.3Mg and (Sn40Bi)0.5Al were cast into 2 mm diameter rod. The solder rod was cut to standard weight of 0.10 gram in granule form. Soda-lime-silica glass as the substrate was prepared by cutting 2 mm thick glass panel into 33 x 16 mm plate. Sn5Sb1.2Cu substrate was alloyed by adding Cu and Sb into molten Sn and cast into sheet form. The sheet was rolled to 2 mm thick and cut to 55 x 20 mm plate. Solder alloys (Sn40Bi)0.3Mg and (Sn40Bi)0.5Al were cast into 2 mm diameter rod. The solder rod was cut to standard weight of 0.10 gram in granule form. Soda-lime-silica glass as the substrate was prepared by cutting 2 mm thick glass panel into 33 x 16 mm plate. Sn5Sb1.2Cu substrate was alloyed by adding Cu and Sb into molten Sn and cast into sheet form. The sheet was rolled to 2 mm thick and cut to 55 x 20 mm plate.

US was conducted with glass and Sn5Sb1.2Cu plates arranged in lap joint position. The plates were clamped in a fabricated soldering apparatus as shown in Figure-1. Soldering temperature was set to 150 °C by a 150 W electrical heater fixed to the apparatus. Lower setting inhibits solder flow while higher setting delays solidification. Glass surface was cleaned with petrol and cloth before placement to the apparatus. US was conducted using a soldering device 'Sunbonder USM-5' from Kuroda Technology at frequency of 60 kHz. Glass surface was roughened by manually rubbing soldering tool tip at 450 °C. Vibration power was set at 2, 4, 6, 8, 10 and 12 Watts. Durations of roughening time were at 1, 2, 3 and 4 minutes per segment. Altogether 24 samples for each solder alloy were tested. Another set of samples for each solder alloy was tested without roughening process. Glass surface roughness was measured using Mitutoyo surface roughness measurement Surftest before placement back into the apparatus. Oxide layer on the sides of Sn5Sb1.2Cu plate was scrapped by knife before placement into the apparatus. Heating system was activated and upon reaching 150 °C, solder granule was placed on glass surface. US parameters were set at tool tip temperature of 450 °C and vibration power of 8W. Solder granule melted upon contact with tool tip. The molten solder was rubbed by vibrating tool tip vigorously on glass surface and the edge of Sn5Sb1.2Cu plates for 30 seconds. The steps were repeated on the 2nd segment. Heating was switch off and soldered specimen removed upon reaching room temperature. Measurements were based on the average of 4 replications. Glass soldered surface area is at 1.12 cm^2 while the soldered surface area at the edge of Sn5Sb1.2Cu plate is at 0.64 cm^2.

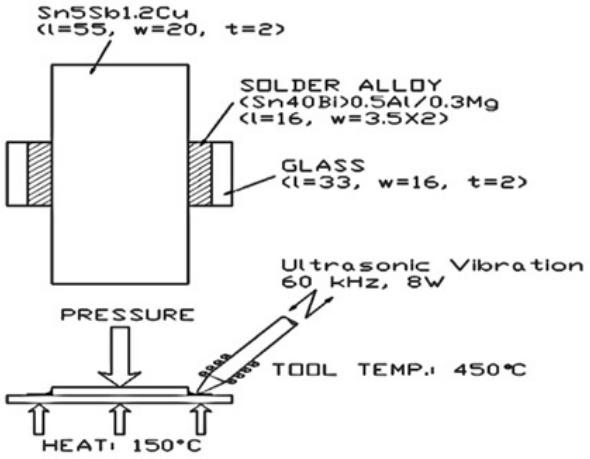

Figure-1. Schematic diagram of soldering apparatus.

The fabricated apparatus shown in Figure-2 was utilized for tensile test. The soldered specimen was clamped within the apparatus and placed in Instron 5582 tension testing machine. Rate of tensile test was fixed at 2 mm/ min. Test was conducted at room temperature. Measurements of shear separation force were based on the average values of 4 replications.

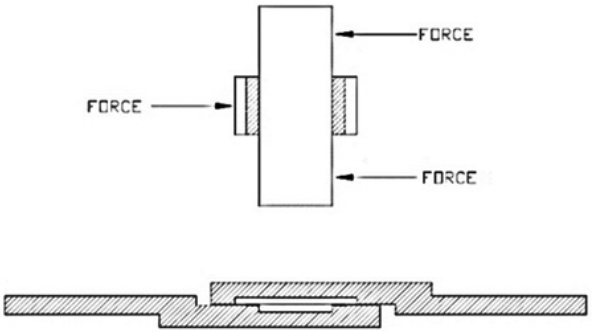

Figure-2. Schematic diagram of tensile test apparatus.

Characterization on solder joint was conducted only between glass and both solders as fracture was not detected between solders and Sn5Sb1.2Cu. SEM on solder joints was conducted using JEOL JSM-6700F at 2000x magnifications. EDX analysis to determine the elements wt% was conducted using JEOL JSM-5600 at 15.0 KV. The elements measured were Sn, Bi, Mg, Al, Si, Na and Ca. Measurements were taken starting from interface. Locations of measurement were expanded at intervals of 10 μm from interface toward both sides of the glass and solders regions until the readings stabilized.

RESULTS AND DISCUSSION

Glass surface roughness prior to roughening was measured at 0.02 μm. Surface roughening produced variable glass surface roughness Ra ranging from 0.08 to 0.30 μm. Optical microscope sample photos of glass with variable surface roughness are shown in Figure-3.

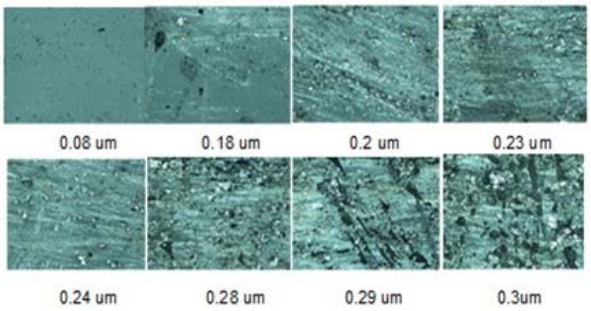

Figure-3. Photos of glass surfaces at variable surface roughness.

The graph of glass surface roughness against vibration power and roughening is shown in Figure-4. Rough glass surface was obtained from roughening through variable vibration power, ranging from 2 -12 W and roughening time of 1 – 4 minutes per segment. Surface roughness peaked at vibration power of 10 W. Higher vibration amplitude caused the flattening of glass surface with reduction in surface roughness. Surface roughness also peaked at 4 minutes duration of roughening. Increasing the duration may increase the surface roughness but is not cost effective.

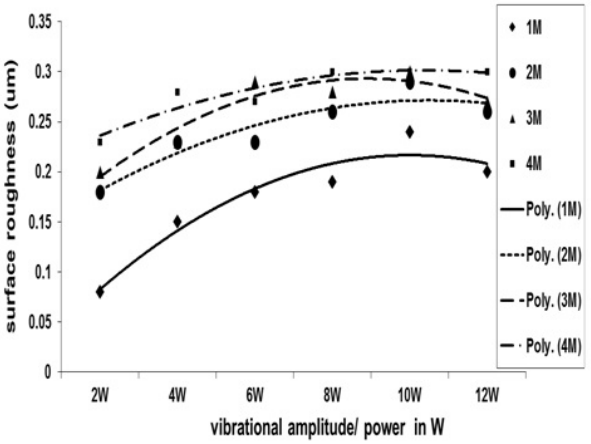

Figure-4. Glass surface roughness against vibration power and roughening time.

Tensile test was used to determine the shear force required to separate the soldered specimen of glass and Sn5Sb1.2Cu. The graph of shear separation force in kN and extension before fracture graph in mm based on a sample specimen is shown in Figure 5. Solder fractures were observed occurring only between solders and glass and not between Sn5Sb1.2Cu and solders. Bond between solders and glass with larger soldering surface area of 1.12 cm^2 was weaker than metallic bond between solders and Sn5Sb1.2Cu with soldering surface area at 0.64 cm^2.

Shear separation strength

Shear separation strength was obtained by dividing shear separation force from the tensile test with soldered surface area at 1.12 cm^2. Shear separation strength is equivalent to the adhesion strength between glass and solders. The graph of shear separation strength against surface roughness for both solder alloys is shown in Figure-6. Shear separation strength for both solders improved with increasing glass surface roughness. Rougher surfaces provided catchment points for stronger adhesion of solders to glass. Shear separation strengths for (Sn40Bi)0.3Mg were stronger than (Sn40Bi)0.5Al at Ra of 0.02 - 0.13 µm. At Ra of 0.13 - 0.30 µm, shear separation strengths of (Sn40Bi)0.5Al were stronger than (Sn40Bi)0.3Mg. Increasing surface roughness from 0.02 to 0.30 µm improved shear separation strength by 34% for (Sn40Bi)0.3Mg and 125% for (Sn40Bi)0.5Al. Based on the graph, the average shear separation strength values peaked at 3.90 MPa for (Sn40Bi)0.3Mg and 4.53 MPa for (Sn40Bi)0.5Al. For comparison, the separation strength of 2.90 MPa were obtained on Zn based solders [13].

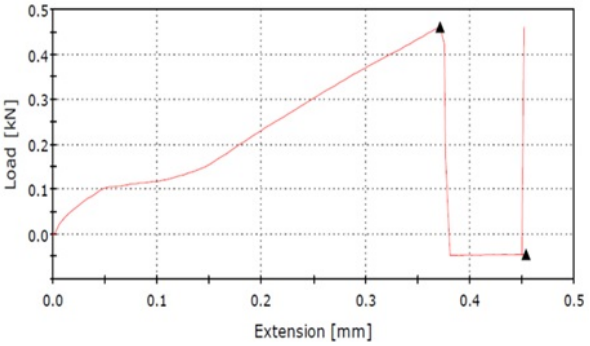

Figure-5. Sample graph for one specimen of shear separation force and extension before fracture.

Extension before fracture

The graph of extension before fracture against surface roughness for both solder alloys is shown in Figure-7. Based on data from Table-1, tensile strength and elongation for (Sn40Bi)0.5Al are at 70.6 MPa and 5.40 %. Tensile strength and elongation for (Sn40Bi)0.3Mg solder are higher at 77.15 MPa and 6.18 %. The extension before fracture for (Sn40Bi)0.5Al solder alloy decreased with increasing glass surface roughness. At low surface roughness, the solders came off from glass completely in single piece. The single piece separation resulted in longer extension before fracture of the solders. At mid-level surface roughness, solders separated from glass in medium sized pieces leaving patches behind. The extension of solders before fracture values were at medium level due to partial breakage. At high glass surface roughness, solders broke off leaving large patches stuck on glass. Few glass specimens broke off completely. The abrupt fractures resulted in lower extension before fracture values. At low surface roughness, (Sn40Bi) 0.3Mg solders came off completely in single piece, resulting in higher extension before fracture values. At mid-level, the extension before fracture values dipped with the solders separating from glass in medium sized pieces. The extension before

fracture values increased at high surface roughness. This is due to higher tensile strength and elongation for (Sn40Bi) 0.3Mg despite the solders breaking off and leaving large patches on glass.

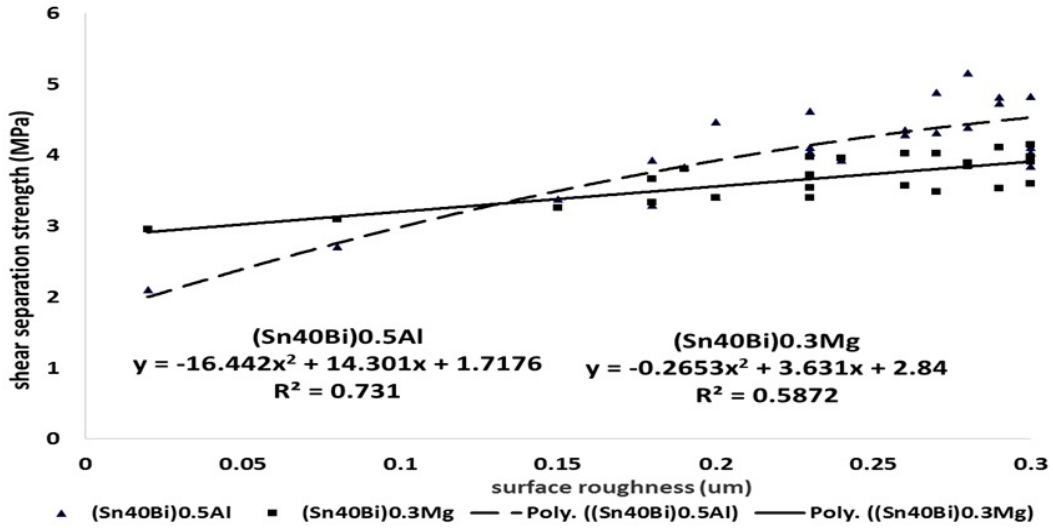

Figure-6. Shear separation strength against surface roughness for (Sn40Bi)0.5Al and (Sn40Bi)0.3Mg.

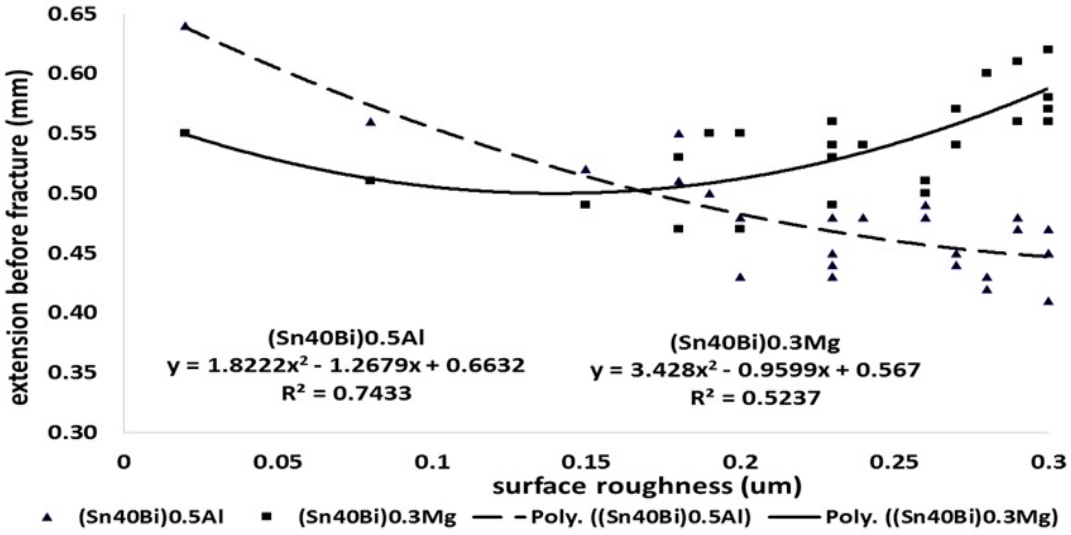

Figure-7. Extension before fracture against surface roughness for (Sn40Bi)0.5Al and (Sn40Bi)0.3Mg.

Characterization of solder joint

SEM analysis was conducted on the joint between glass and both solder alloys (Sn40Bi)0.5Al and (Sn40Bi)0.3Mg. Both glass samples had surface roughness of 28 µm. The SEM micrograph for (Sn40Bi)0.5Al conducted at 2000 magnifications is shown in Figure 8. There was no visible formation of intermetallic compound layer. The SEM micrograph for (Sn40Bi)0.3Mg conducted at 2000 magnifications is shown in Figure 9. Similarly, there was no visible formation of intermetallic compound layer. The absence of IMC layer for both solder alloys signifies that the bonding mechanism is not based on diffusion of solders into the interface with the substrates. Molten (Sn40Bi)0.5Al solders bonded to both flat surface and the crevices created by surface roughening of the glass. Gaps were visible especially on flat surfaces between glass and both solders. The numerous gaps signify incomplete bonding. Molten (Sn40Bi)0.3Mg solders also bonded to both flat surface and the crevices created by surface roughening of the glass. The lesser gaps signify a more complete bonding. (Sn40Bi)0.3Mg had stronger shear separation strength on smoother surface than (Sn40Bi)0.5Al, as seen in Figure-6.

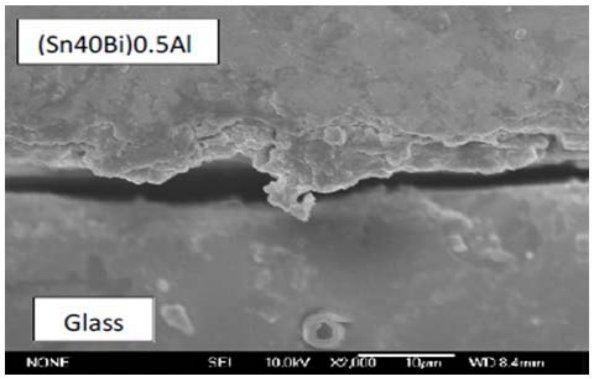

Figure-8. SEM micrographs at 2000x magnifications of joint between (Sn40Bi)0.5Al solders and glass.

Both molten solder alloys flowed and solidified in the glass crevices forming protrusions adhering to glass. The protrusions formed mechanical adhesion. Deeper crevices from higher surface roughness formed larger protrusions and stronger adhesion.

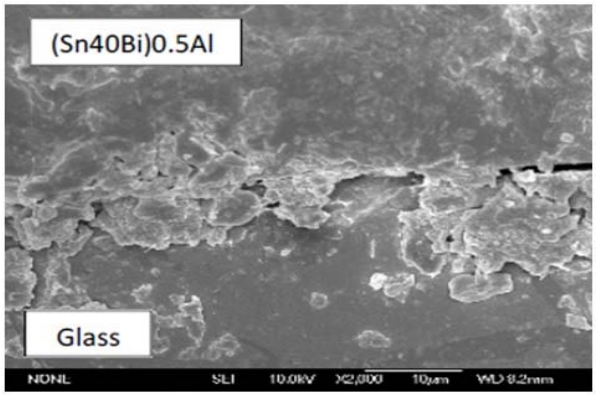

Figure-9. SEM micrographs at 2000x magnifications of joint between (Sn40Bi)0.3Mg solders and glass.

EDX analysis was conducted on the interface between glass and solders. First measurement of the elements by wt% was conducted at the interface. Subsequent measurements covered up to 40 μm at intervals of 10 μm from the interface within both solders and glass regions. The elements by wt% had stabilized at 40 μm from interface. The graphs for elements by wt% against distance from interface are shown in Figure-10 for (Sn40Bi) 0.5Al and Figure-11 for (Sn40Bi)0.3Mg.

Sn, Bi and Al_2O_3 (alumina) were detected on the solders side of (Sn40Bi)0.5Al. Sn, Bi and MgO (magnesia) were detected on the solders side of (Sn40Bi)0.3Mg. Sn and Bi for both solder alloys remained in metallic form without oxidation. Based on US test conducted by the author, both Sn and Bi did not adhere to glass. Sn moved up to 20 μm beyond the interface while Bi migrated deeper than 40 μm into the glass region. Al from (Sn40Bi)0.5Al passivated into Al_2O_3. Al forms passivation layer of Al_2O_3 as a reaction with atmospheric oxygen [14]. Al_2O_3 from solders migrated 20 μm beyond the interface becoming bonding agent of solders to glass. Mg from (Sn40Bi)0.3Mg passivated into MgO. Mg in air forms instantaneous passivation 25nm thick layer of MgO [15, 16]. MgO from solders migrated 10 μm beyond the interface becoming bonding agent of solders to glass.

SiO_2 (silica), Na_2O (sodium oxide), CaO (lime), MgO and Al_2O_3 were detected in glass region prior to soldering. After soldering, only SiO_2 which is the main constituent of glass moved in larger quantity beyond 40 μm into the solders region. SiO_2 is the likeliest bonding agent within glass. Na_2O was also detected within solders region in smaller quantity. However, it's unlikely to be the bonding agent due to its main role as agent for reducing the transition temperature of glass. Both Al_2O_3 and MgO from glass remained within the glass region up to the interface and did not play a role as bonding agent.

[17] concluded that solder bond between ceramic and solder is through surface energy and metal oxide adhesions. Research by [13] strongly suggested that chemical bond between glass plate and SnZn is 'Zn-O-Si' with Si being the bonding agent for glass. Surface energy can be discounted for adhesion to glass surface. The possible metal oxide bond between (Sn40Bi)0.3Mg and glass is 'Mg-O-Si' while the bond for (Sn40Bi)0.5Al and glass is 'Al-O-Si'.

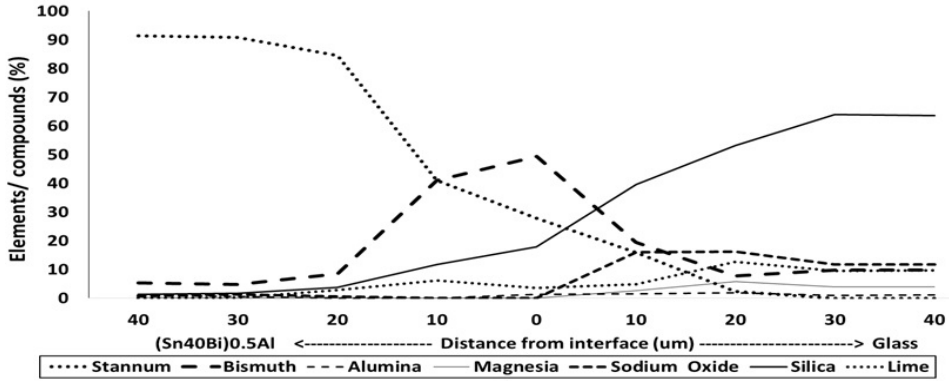

Figure-10. Elements at intermediate region between glass and (Sn40Bi)0.5Al solders.

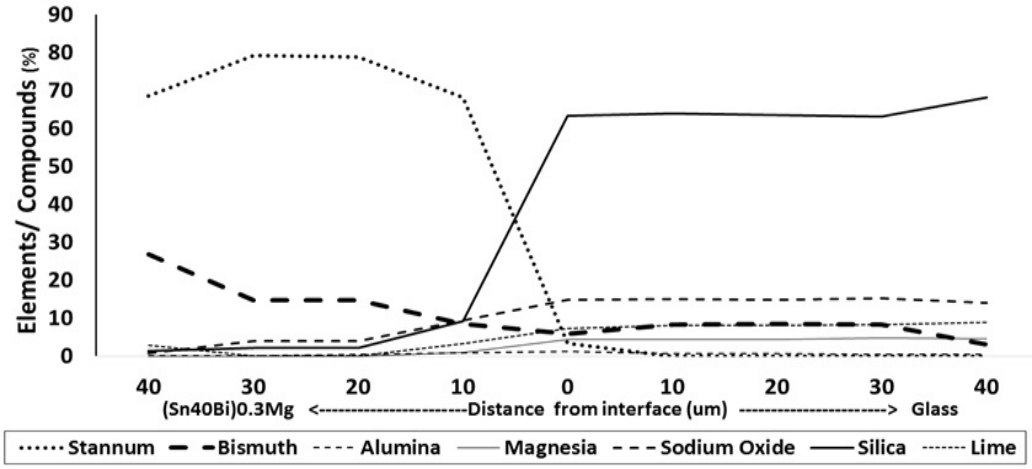

Figure-11. Elements at intermediate region between glass and (Sn40Bi)0.3Mg solders.

Shear separation energy

Shear separation energy is the energy required to separate soldered specimens of glass and Sn5Sb1.2Cu. It is calculated based on Equation (1).

$$Wsep = (Fn/ An) \times Exn \times 0.5) \quad (1)$$

Wsep denotes shear separation energy, Fn/ An denotes shear separation strength and Exn is the extension before fracture. The graph on the relationships between shear separation energy against surface roughness for both solder alloys is shown in Figure-12.

Equation (2) and Equation (3) were empirically derived from the graph in Figure-12 to represent the relationships between shear separation energy (Wsep) and glass surface roughness (Ra). Equation (2) represents (Sn40Bi)0.5Al and Equation (3) represents (Sn40Bi)0.3Mg.

$$Wsep_{(Al)} = -3284Ra^2 + 2299Ra + 613 \text{ J/m}^2 \quad (2)$$

$$Wsep_{(Mg)} = 6418Ra^2 - 845Ra + 821 \text{ J/m}^2 \quad (3)$$

Shear separation energy for both alloys improved with increasing glass surface roughness. There is no additional energy input with the exception of work required to roughen glass surface. Bond between glass and solders consists of metal oxide adhesion and mechanical adhesion. Metal oxide adhesion is the soldering bond when surface roughness of glass is theoretically at zero. Mechanical adhesion is the additional adhesion contributed by the increasing glass surface roughness. The approximate values of metal oxide adhesion and mechanical adhesion for the bonding between glass and the respective solder alloys can be derived from Equation (2) and Equation (3). The values are dependent on surface roughness Ra. Increasing surface roughness from theoretical value of 0.00 μm to 0.30 μm improved shear separation energy by 64% for (Sn40Bi)0.5Al and 39% for (Sn40Bi)0.3Mg.

(Sn40Bi)0.5Al solders and glass with Ra of 0.30 μm;
Metal oxide adhesion = 613 J/m^2
Mechanical adhesion = 394 J/m^2
Shear separation energy $Wsep_{(Al)}$ = 1007 J/m^2
(Sn40Bi)0.3Mg solders and glass with Ra of 0.30 μm;
Metal oxide adhesion = 821 J/m^2
Mechanical adhesion = 324 J/m^2
Shear separation energy $Wsep_{(Mg)}$ = 1145 J/m^2

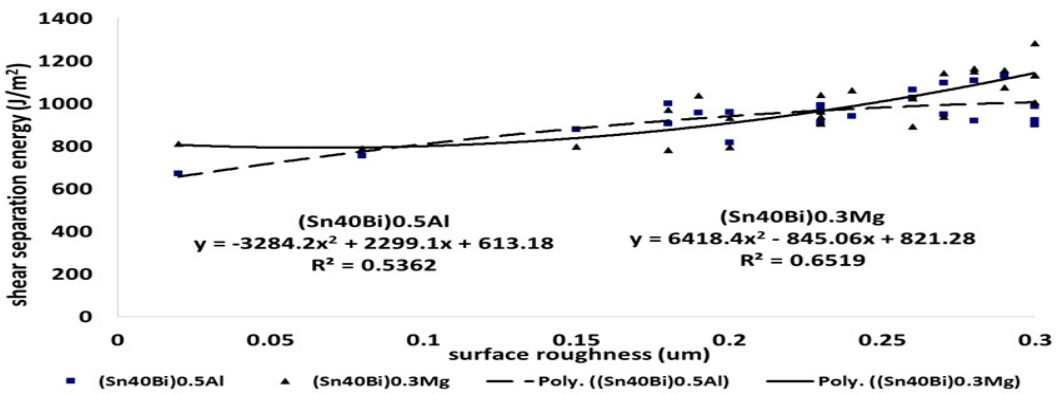

Figure-12. Shear separation energy against surface roughness for (Sn40Bi)0.5Al and (Sn40Bi)0.3Mg solders.

Shear separation strength for (Sn40Bi)0.3Mg solders with bond of Mg-O-Si was stronger at lower glass surface roughness than (Sn40Bi)0.5Al solders with bond of Al-O-Si. Heat, pressure and ultrasonic vibration during US caused imperfect bonding between oxygen atoms of MgO with SiO_2 and also between Al_2O_3 with SiO_2. MgO has lower bond dissociation energy of 358 kJ/mol when compared to Al_2O_3 at 502 kJ/mol. The lower bond dissociation energy for ionic MgO resulted in weaker pull of oxygen by Mg. The weaker pull created stronger Mg-O-Si imperfect bonding of oxygen atoms with SiO_2. The reverse is true for Al-O-Si bond involving Al_2O_3 with SiO_2. The bond dissociation energies data is shown in Table-2.

Table-2. Bond dissociation energies in diatomic molecules [18].

Materials	Bond dissociation energies (kJ/mol)
Al-O	501.9±10.6
Mg-O	358.2±7.2
Si-O	799.6±13.4

At higher surface roughness, glass surfaces have deeper and greater crevices allowing for formation of larger protrusions from flowing molten solders. The passivated metal oxides migrated and formed the outer surface of the protrusions. Metal oxides with greater fracture toughness are more difficult to break during separation by tensile test. Fracture toughness for Al_2O_3 is at 4 $MPa.m^{1/2}$ and MgO is at 2.8 $MPa.m^{1/2}$ as shown in Table-3. This resulted in stronger mechanical adhesion and shear separation strength for glass to (Sn40Bi)0.5Al when compared to glass and (Sn40Bi)0.3Mg at higher surface roughness.

Table-3. Fracture toughness data for metal oxides, Al_2O_3 [19] and MgO [20].

Materials	Maximum fracture toughness (M Pa ^{½})
Al_2O_3	4.0
MgO	2.8

CONCLUSIONS

Study on the effect of surface roughness on adhesion strength in ultrasonic soldering of glass reached the following conclusions.

i. The combination of metal oxide adhesion and mechanical adhesion formed the bond between glass and (Sn40Bi)0.3Mg and (Sn40Bi)0.5Al solder alloys. Metal oxide adhesion predominates at lower surface roughness. Proportion of mechanical adhesion increases with higher surface roughness.

ii. Metal oxide adhesion with glass is in the form of Mg-O-Si for (Sn40Bi)0.3Mg and Al-O-Si for (Sn40Bi)0.5Al. Metal oxide adhesion is stronger for Mg-O-Si than Al-O-Si due to weaker ionic bond of MgO resulting in stronger Mg-O-Si bond.

iii. Mechanical adhesion is stronger at rougher glass surface for (Sn40Bi)0.5Al than (Sn40Bi)0.3Mg solders. Passivated layer of Al_2O_3 forming protrusions within glass crevices has higher fracture toughness and more difficult to break than passivated layer of MgO.

iv. Shear separation strength between glass and both solders improved with increasing glass surface roughness from 0.02 µm to 0.30 µm. Improvements achieved were 34% for (Sn40Bi)0.3Mg and 125% for (Sn40Bi)0.5Al.

v. Shear separation energy between glass and both solders improved with increasing glass surface roughness from theoretical value of 0.00 µm to 0.30 µm. Improvements achieved were 39% for (Sn40Bi)0.3Mg and 64% for (Sn40Bi)0.5Al.

ACKNOWLEDGEMENTS

The authors are grateful to Agile and Sustainable Manufacturing Research Unit (ASMARU) of International Islamic University of Malaysia and Royal Selangor International for the support given in this research.

REFERENCES

[1] Xu Z., Ma L., Yan J., Yang S. and Du S. 2000. Wetting and oxidation during ultrasonic soldering of an alumina reinforced aluminum–copper– magnesium (2024 Al) matrix composite. Composites: Part A, Vol. 43, pp. 407–414.

[2] Nagaoka T., Morisada Y., Fukusumi M. and Takemoto T. 2011. Selection of soldering temperature for ultrasonic-assisted soldering of 5056 aluminum alloy using Zn–Al system solders. Journal of Materials Processing Technology, Vol. 211, No. 9, pp. 1534–1539.

[3] Nagaoka T., Morisada Y., Fukusumi M. and Takemoto. T. 2010. Ultrasonic-Assisted Soldering of 5056 Aluminum Alloy Using Quasi-Melting Zn-Sn Alloy. Metallurgical and Materials Transactions B: Process Metallurgy and Materials Processing Science, Vol. 41, No. 4, pp. 864-871.

[4] Li Y.X., Leng X.S., Cheng S. and Yan J.C. 2012. Microstructure design and dissolution behavior between 2024 Al/Sn with the ultrasonic-associated soldering. Materials and Design, Vol. 40, pp. 427–432.

[5] Nagaoka T., Morisada Y., Fukusumi M. and Takemoto. T. 2009. Joint strength of aluminum ultrasonic soldered under liquidus temperature of Sn–Zn hypereutectic solder. Journal of Materials Processing Technology, Vol. 209, pp. 5054–5059.

[6] Yamada M., Nobuhiko C. and Takayuki. M.

2009.Solder Alloy For Bonding Oxide Material, And Solder Joint Using The Same. (Patent application number: 20090104071).

[7] Kim W.C., Lee K.W., Saarinen I.J., Pykari L. and Paik, K.W. 2012. Ultrasonic Bonding of Anisotropic Conductive Films Containing Ultra fine Solder Balls.

[8] for High-Power and High-Reliability Flex-On-Board Assembly IEEE Transaction on Components, Packaging and Manufacturing Technology, Vol. 2, No. 5.

[9] Lee K.W., Saarinen I.J., Pykari L. and Kyung W.P. 2011. High Power and High Reliability Flex-On-Board Assembly Using Solder Anisotropic.

[10] Conductive Films Combined with Ultrasonic Bonding Technique. IEEE Transaction on Components, Packaging and Manufacturing Technology, Vol. 1, No. 12.

[11] Tamuraa S., Tsunekawa Y., Okumiya M. and Hatakeyama, M. 2008. Ultrasonic cavitation treatment for soldering on Zr-based bulk metallic glass. Journal of Materials Processing Technology, Vol. 206, pp. 322–327.

[12] Li Y.X., Zhao W.W., Leng X.S., Fu Q.J., Wang L. and Yan, J.C. 2011. Microstructure evolution and mechanical properties of ultrasonic-assisted soldering joints of 2024 aluminium alloys. Trans. Non ferrous Met. Soc. China, Vol. 2, pp. 1937 –1943.

[13] Ding M., Zhang P.L., Zhang Z.Y. and Yao S. 2010. A novel assembly technology of aluminum alloy honeycomb structure, Int J Adv Manuf Technol, Vol. 46, pp. 1253–1258.

[14] Mei Z. Q., Holder H. A. and Vander Plas H. A. 1996. Low-Temperature Solders August 1996 Hewlett-Packard Journal Article, Vol. 10.

[15] Yonekura D., Ueki T., Tokiyasu K., Kira S. and Wakabayashi, T. 2014. Bonding mechanism of lead-free solder and glass plate by ultrasonic assisted soldering method. Materials and Design, Vol. 65, pp. 907-913.

[16] Ekuma C.E., Idenyi N.E. and Umahi A.E. 2007. The effects of zinc additions on the corrosion susceptibility of aluminum alloys in various tetraoxosulphate (VI) acid environments. Journal of Applied Sciences, No. 2, pp. 237-241.

[17] Ono, S. 1998. Surface phenomena and protective film growth on magnesium and magnesium alloys Metallurgical Science and Technology Vol. 16, No.2.

[18] Diler E., Lescop B., Rioual S., Nguyen Vien G., Thierry D. and Rouvellou B. 2014. Initial formation of corrosion products on pure zinc and $MgZn_2$ examinated by XPS. Corrosion Science, Vol. 79, pp. 83-88.

[19] Finnis M.W. 1996. The theory of metal–ceramic interfaces J. Phys.: Condens. Matter, 8: 5811–5836.

[20] Lou, Y. R., 2010. Bond dissociation energies http://staff.ustc.edu.cn/~luo 971/2010-91-CRC-BDEs-Tables.pdf (accessed 17 September 2015).

[21] Accuratus: aluminum oxide properties http://accuratus. com/alumox.html (accessed 25 February 2015)

[22] Azo Materials: Magnesia - Magnesium Oxide (MgO) Properties & Applications http:// www.azom. com/properties.aspx?ArticleID=54 (accessed 25 February 2015).